ASSESSMENT OF LIGHT ENVIRONMENT FOR HERBACEOUS VEGETATION IN SEMI-NATURAL GRASSLAND USING TIME-SERIES UAV DATA

Naoko Miura[1]*, Yuji Niwa[1], Susumu Yamada[2]

[1]Graduate School of Agricultural and Life Sciences, the University of Tokyo – 1-1-1 Yayoi, Bunkyo-ku, Tokyo 113-8657 Japan, miura@uf.a.u-tokyo.ac.jp, uz28@uf.a.u-tokyo.ac.jp
[2] Faculty of Agriculture, Tokyo University of Agriculture – 1737 Funako, Atsugi-shi, Kanagawa 243-0034 Japan, sy206447@nodai.ac.jp

KEY WORDS: UAV, light environment, herbaceous vegetation, semi-natural grassland, gap fraction, NDVI, solar radiation

ABSTRACT:

Grasslands are important ecosystems containing unique biodiversity. It has been reported that some herbaceous species inhabiting grassland reduced its number and became extremely rare. Restoring these species as well as maintaining the grassland are key issues. Light environment is crucial for plant growth and survival. It is particularly important to evaluate light environment of microsite for herbaceous vegetation. In this paper, NDVI, vegetation biomass and gap fraction were estimated using time-series UAV data, and compared to photosynthetic photon flux density (PPFD), solar radiation and gap fraction measured by traditional ground-based techniques to validate its utility in accessing light environment for herbaceous vegetation in semi-natural grassland. The results showed that UAV derived variables displayed overall good correlations with ground derived variables: relative PPFD, relative solar radiation and gap fraction. Analysis of time-series UAV data revealed that UAV derived NDVI and vegetation biomass were not suitable for evaluating light environment when vegetation attains its maturity. UAV derived gap fraction was most resilient to change of vegetation growth. UAV derived methods have advantage in evaluating light environment in microsite without disturbing valuable plants and would help restoring semi-natural grassland.

1. INTRODUCTION

Grasslands are important ecosystems containing unique biodiversity. In Japan, grassland of *Miscanthus sinensis*, which is a tall, perennial grass species and characterized by erect and tufted forms (Hayashi et al., 1981), has been one of the symbolic landscapes. It is a semi-natural grassland and requires controlled burn to maintain the grassland, however, local communities are increasingly shorthanded for controlled burn these days (Takahashi, 2019). It has been reported that some herbaceous species inhabiting grassland reduced its number and became extremely rare (Nebara-District and Asagiri-Highlands-Revitalization-Committee, 2018). Restoring these species as well as maintaining the grassland are key issues.

Light environment is crucial for plant growth and survival. It is particularly important to evaluate light environment of microsite for herbaceous vegetation. Ground-based techniques to access light condition have been commonly used. A light sensitive film is one of the traditional techniques. A color acetate film is exposed, and the absorbance of the dye gradually fades. The rate of fading associates well with solar radiation and photosynthetic photon flux density (PPFD) which plays an important role in the growth and survival of photosynthetic organisms. The film has been used in measuring solar radiation, for example, for soybean (Kumagai, 2018) and grapevine (Bontempo et al., 2018) . Light sensors can directly measure PPFD and used in many studies (e.g. Flanagan et al., 2002; Tang et al., 1989), although they are more expensive equipment compared to a simple film. Other method to access light environment is to compute gap fraction, which is defined as the fraction of sky visible through the canopy (Welles and Norman, 1991), using fisheye camera. This method has been widely used in forest (e.g. Pinag¨¦ et al., 2014; Macfarlane et al., 2007) and can be applied to grassland.

The recent development of unmanned aerial vehicle (UAV) technology has shown great potential to study grasslands, since it can acquire data more frequently with higher spatial resolution (in the order of centimetres) in cost-effective manner, compared to the conventional airborne data acquisition by airplane. It is a non-destructive method to derive plant parameters in large area. Using UAV imagery with a combination of structure from motion (SfM) and multi-view stereo (MVS) technique, grassland biomass has been successfully estimated in numerous papers (e.g. Miura et al., 2020; Lussem et al., 2019; Grüner et al., 2019). Normalized difference vegetation index (NDVI) is a common and widely used remote sensing index which quantifies vegetation greenness. NDVI derived from multispectral sensor boarded on UAV has been extensively used in agriculture (e.g. Matese and Di Gennaro, 2021; Hassan et al., 2019). Both vegetation biomass and NDVI has potential for evaluating light environment in grassland. Gap fraction or fractional cover has been successfully estimated in forest environment by LiDAR boarded on airplane. Fractional cover was derived as the ratio of canopy returns to the total number of returns per unit area (Næsset, 1997). Similar methods utilising the point density of LiDAR returns to estimate fractional cover were presented in other studies (e.g. Coops et al., 2007; Hopkinson and Chasmer, 2007; Morsdorf et al., 2006). Although traditional LiDAR cannot be applied to grassland because of low spatial resolution and point density, point cloud derived from UAV LiDAR or UAV

* Corresponding author

imagery with a combination of SfM and MVS would satisfy the requirement for analysis of herbaceous vegetation. The SfM point cloud is successfully used to derive structural parameters of crops (e.g. Zhang et al., 2021; Santos et al., 2020) and better in terms of cost than UAV LiDAR. The SfM point cloud can be applied to estimate gap fraction in grassland.

In this paper, NDVI, vegetation biomass and gap fraction were estimated using time-series UAV data, and compared to PPFD, solar radiation and gap fraction measured by traditional ground-based techniques to validate its utility in accessing light environment for herbaceous vegetation in semi-natural grassland. We use time-series UAV data, which covers growing season of vegetation in the study area, because growth stage of vegetation may have an impact on the analysis (Miura et al., 2020).

2. METHODS

2.1 Study area

The Study area locates in Nebara district, Asagiri Highlands at the western foot of Mt. Fuji in Shizuoka Prefecture, Japan (138°35'47.133"E 35°25'32.151"N, Figure 1). The elevation ranges from 926 m to 977 m above sea level. Mean annual precipitation and temperature are 2249 mm and 10.6 °C, at the nearby Shiraito Meteorological Station and Kawaguchi-ko Meteorological Station respectively. Grassland which mainly consists of *M. sinensis* spreads over a plateau of lava where complex topography was formed. Nebara district is a famous field of *M. sinensis*, which is used for repairing roof of cultural assets, and registered in 2012 by Agency for Cultural Affairs, Government of Japan as an important area to conserve materials used for cultural properties. The grassland is burnt annually in April to produce good quality *M. sinensis*. After the burn, *M. sinensis* grows until it attains maturity in September. Then, it withers in the next couple of months and is finally harvested during winter before the annual control burn is conducted in the next April. In the grassland, rare and important herbaceous vegetation such as *Viola orientalis* inhabits, however, some species such as *Hemerocallis citrina* Baroni var. *vespertine* have reduced their number recently (Nebara-District and Asagiri-Highlands-Revitalization-Committee, 2018; Yuasa et al., 2002).

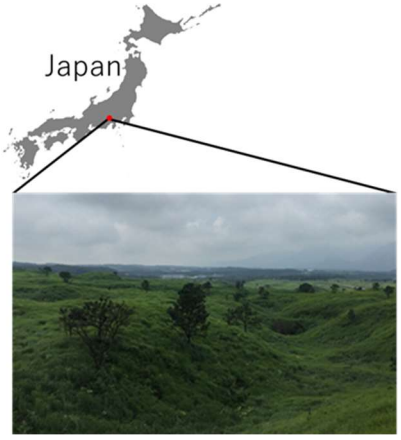

Figure 1. Study area.

2.2 Ground survey

Ground survey was conducted on May 30-31, June 28-30 and August 25-26. Through this period, vegetation grows and attains maturity. A rectangular plot, which is approximately 10 m by 10 m, was set up in north and south area respectively. In the plot, 9 measurement points were set up at the intersections of squares divided into 16 parts. Measurement for PPFD, solar radiation and gap fraction was conducted at a hight of 20 cm from the ground at each measurement point (Figure 2). The height was selected to access light environment for vegetation species in the low layer of *M. sinensis* community. Nemoto (2010) divided species of *M. sinensis* community into 3 hight layers: top (higher than 151 cm), intermediate (between 51cm and 150 cm) and low (lower than 50 cm). The low layer includes *Viola* species which is one of the targeted species in this study.

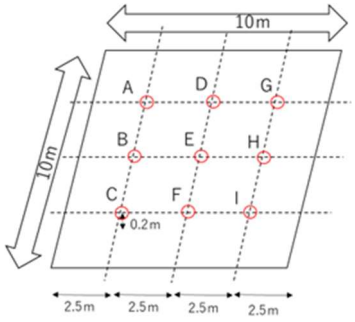

Figure 2. Plot design.

2.2.1 Relative photosynthetic photon flux density: PPFD was measured using LI-COR light sensor LI-250 and LI-190SA. Measurement was conducted at 9 measurement points and outside of the plot, where the sun light was unobstructed, for 15 seconds respectively. The values were averaged at each measurement point. These values were then divided by the value outside of the plot to compute relative photosynthetic photon flux density (RPPFD). The value is expressed as percentage. The reason to compute RPPFD instead of using the raw value of PPFD is to monitor and compare how much PPFD is received at each measurement point compared to PPFD under full sunlight in the process of vegetation growth.

2.2.2 Relative solar radiation: Solar radiation was measured using light sensitive film, Optoleaf (Taisei Fine Chemical Co., Ltd.). Three pieces of the film were set up at the measurement points (Figure 3) and outside of the plot where the sun light was unobstructed. The films were exposed for 19 to 45 hours. The degree of absorbance was measured before and after the exposure using a portable photometer, D-Meter RYO-470M (Taisei Fine Chemical Co., Ltd.). Color fade rate was calculated dividing the degree of absorbance after the exposure by that before the exposure. The values of 3 films at each measurement point were averaged. The integrated amount of solar radiation was calculated utilizing OptoLeaf color fade curves provided by the manufacturer (Taisei Fine Chemical Co.). Solar radiation S (MJ/m^2) is expressed:

$$S = -1.675\left(\frac{D}{Do} \times 100\right) + 18.23 \qquad (3)$$

where D = Degree of absorbance after exposure
Do = Degree of absorbance before exposure

Relative solar radiation (RS) was calculated dividing solar radiation at each measurement point by that outside of the plot. The value is expressed as percentage.

https://doi.org/10.5194/isprs-annals-X-1-W1-2023-1081-2023

Figure 3. Light sensitive films at a measurement point.

2.2.3 Gap fraction: Gap fraction (GF) was measured using a 360-degree camera, RICOH THETA. Image was captured at each measurement point and transformed to fisheye image of upper hemisphere. In this process, we used the method of Honjo *et al*. (2019). Then, gap fraction was calculated using CanopOn 2 software (Figure 4).

Figure 4. Fisheye image of upper hemisphere at a measurement point.

2.3 UAV data

2.3.1 Data acquisition: UAV data were acquired on April 26, June 1, June 28 and August 25 in 2019. UAV flight in June and August was conducted at the same time with the ground survey. We used DJI Phantom 4 Pro for orthomosaic image, Digital Surface Model (DSM) and point cloud, and Phantom 4 Multispectral for NDVI. Flight altitude was set as 15 m from the ground, which resulted in image data with a ground sampling distance (GSD) of between 0.40 and 0.43 cm for Phantom 4 pro data and of between 0.68 and 0.82 cm for Phantom 4 Multispectral data. Images were captured with 2 seconds shutter interval, and 85%/90% side/forward overlap. Ground control points (GCPs) were set up at 4 places outside of both vegetation plots respectively and GNSS surveyed. Additionally, 4 corners of the vegetation plots were GNSS surveyed as validation points to examine z values of UAV data products. The captured images were processed using SfM + MVS software, Pix4D. For calculation of UAV derived variables, a circular subplot of 1 m radius was defined at the measurement points in each plot (Figure 5).

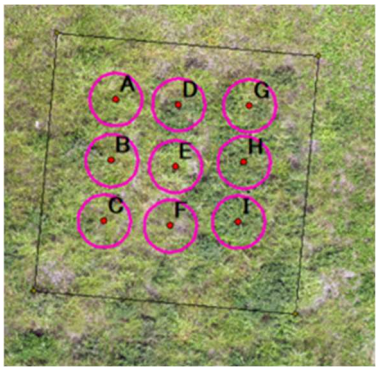

Figure 5. Nine circular subplots of 1 m radius for calculation of UAV derived variables. An ortho mosaic image is August 25 data of the north plot.

2.3.2 Vegetation biomass: Vegetation biomass is calculated using the pixel size and canopy height information in each subplot using the method of Miura *et al.*(2020) where vegetation biomass is calculated as a volume. We used the DSM made from images acquired in April as Digital Terrain Model (DTM), since there was no vegetation on the ground at the time of data acquisition due to annual burning in the area. Canopy height was calculated by subtracting DTM from DSM. This creates Canopy Height Model (CHM). The volume of each subplot in each data acquisition, V is expressed:

$$V = \sum_{i=1}^{n} a^2 h_i \qquad (1)$$

where a = pixel size of each CHM
h = canopy height value of each pixel in each subplot
n = the number of pixels in each subplot

2.3.3 Gap fraction: GF is calculated using the point density of point cloud generated by Pix4D. First, fractional cover is derived as the ratio of canopy points, which is defined as points higher than 20 cm from the ground to the total number of points per subplot area. Then, the value of fractional cover is subtracted from 1. GF is expressed:

$$GF = 1 - \frac{P}{T} \qquad (2)$$

where P= number of points higher than 20cm from the ground in each subplot
T = total number of points in each subplot

2.3.4 NDVI: NDVI is computed as a mean value in each subplot using NDVI images derived from Phantom 4 Multispectral.

These values are compared with the values collected in the ground survey. It is noted that both ground survey and UAV derived variables for A, B, C and F measurement points of the south plot in August data were excluded, because the area around the measurement points were accidentally mowed and altered.

3. RESULTS

3.1 Validation of z values of UAV data

As a result of comparison of z values at 4 corners of the plots between GNSS survey and DTM acquired in April, RMSE was 4.4 cm for the north plot, and 2.5 cm for the south plot.

3.2 Comparison between ground survey data

Ground derived variables: relative photosynthetic photon flux density (G_RPPFD), relative solar radiation (G_RS) and gap fraction (G_GF) showed good and significant correlation among them (Figure 6, 7 and 8). G_RPPFD and G_RS showed good correlation in May 31 data with R^2 value of 0.58 (Figure 6a), and significant correlation in June 28 and August 25 data with R^2 value of 0.82 (Figure 6b) and 0.91 (Figure 6c) respectively. Similar trend was observed between G_RPPFD and G_GF with R^2 value of 0.54 (Figure 7a), 0.79 (Figure 7b) and 0.84 (Figure 7c), and between G_RS and G_GF with R^2 value of 0.58 (Figure 8a), 0.82 (Figure 8b) and 0.91 (Figure 8c).

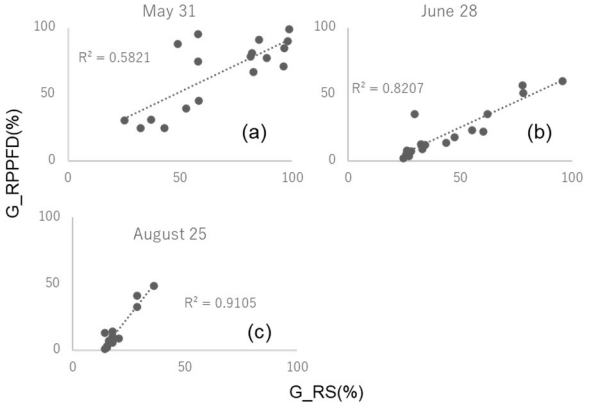

Figure 6. Comparison between ground derived relative photosynthetic photon flux density (G_RPPFD) and relative solar radiation (G_RS): May 31 (a), June 28 (b) and August 25 (c).

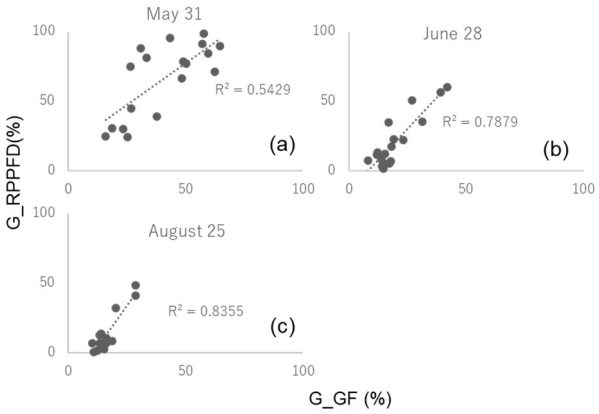

Figure 7. Comparison between ground derived relative photosynthetic photon flux density (G_RPPFD) and gap fraction (G_GF): May 31 (a), June 28 (b) and August 25 (c).

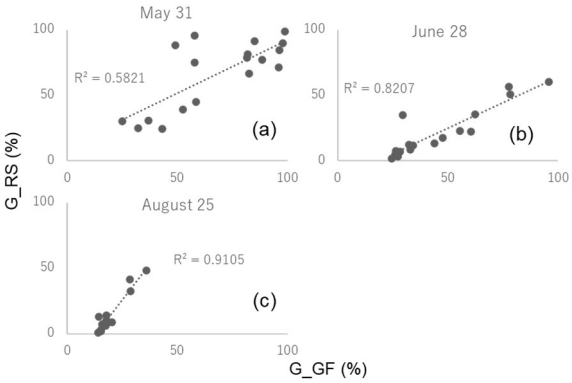

Figure 8. Comparison between ground derived relative solar radiation (G_RS) and gap fraction (G_GF): May 31 (a), June 28 (b) and August 25 (c).

3.3 Comparison between UAV data

UAV derived NDVI (UAV_NDVI) was well correlated with volume (UAV_V) in June 1 and June 28 data with R^2 value of 0.84 (Figure 9a) and 0.69 (Figure 9b), except August 25 data with R^2 value of 0.32 (Figure 9c). UAV_NDVI also displayed significant correlation with UAV derived gap fraction (UAV_GF) with R^2 value of 0.91 (Figure 10a), 0.93 (Figure 10b) and 0.69 (Figure 10c). UAV derived volume (UAV_V) was significantly correlated with UAV_GF in June 1 data with R^2 value of 0.91 (Figure 11a), however, displayed moderate correlation in June 28 and August 25 data with R^2 value of 0.53 (Figure 11b) and 0.49 (Figure 11c).

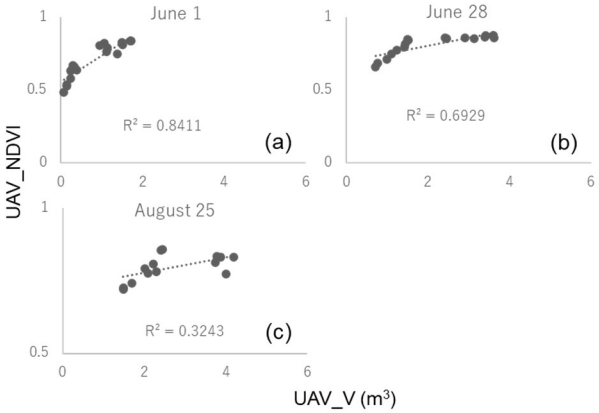

Figure 9. Comparison between UAV derived NDVI (UAV_NDVI) and volume (UAV_V): June 1 (a), June 28 (b) and August 25 (c).

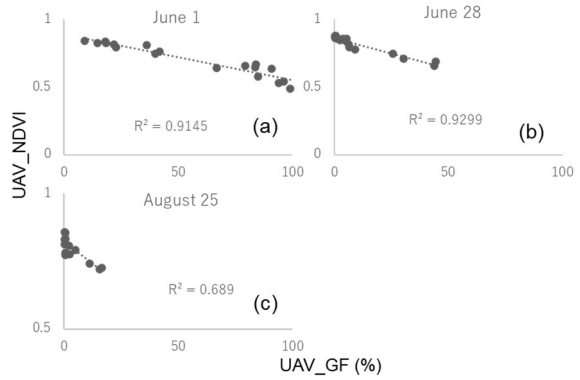

Figure 10. Comparison between UAV derived NDVI (UAV_NDVI) and gap fraction (UAV_GF): June 1 (a), June 28 (b) and August 25 (c).

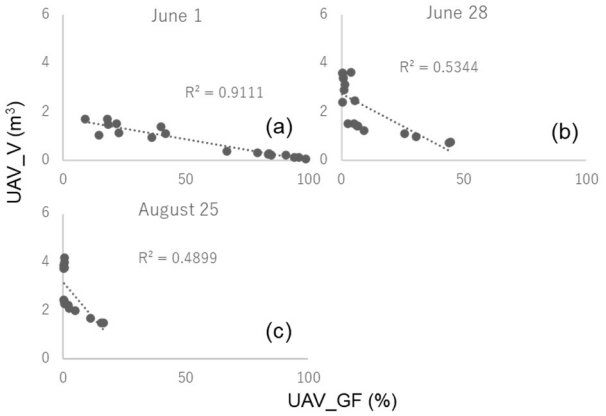

Figure 11. Comparison between UAV derived volume (UAV_V) and gap fraction (UAV_GF): June 1 (a), June 28 (b) and August 25 (c).

3.4 Comparison between ground survey and UAV data

UAV_NDVI presented negative and good correlation with G_RPPFD in June 28 and August 25 data with R^2 value of 0.77 (Figure 12b) and 0.64 (Figure 12c), with G_RS in June 28 data with R^2 value of 0.64 (Figure 12e), and with G_GF in May 31-June 1 and June 28 data with R^2 value of 0.64 (Figure 12g) and 0.62 (Figure 12h). The rest of the data showed moderate correlation (Figure 12a, 12d, 12f and 12i).

UAV_V was negatively associated with ground derived variables. Good correlation was observed with G_RPPFD and G_RS in June 28 data with R^2 value of 0.67 (Figure 13b) and 0.58 (Figure 13e), and with G_GF in May 31-June 1 data with R^2 value of 0.63 (Figure 13g). Other data displayed moderate correlation (Figure 13a, 13c, 13d, 13f, 13h and 13i).

UAV_GF was well correlated with ground derived variables in most data (Figure 14b, 14c, 14e, 14f, 14g, 14h and 14i) displaying R^2 value between 0.6 and 0.8. Only G_RPPFD and G_RS in May 31-June 1 data showed moderate correlation with R^2 value of 0.51 (Figure 14a) and 0.44 (Figure 14d).

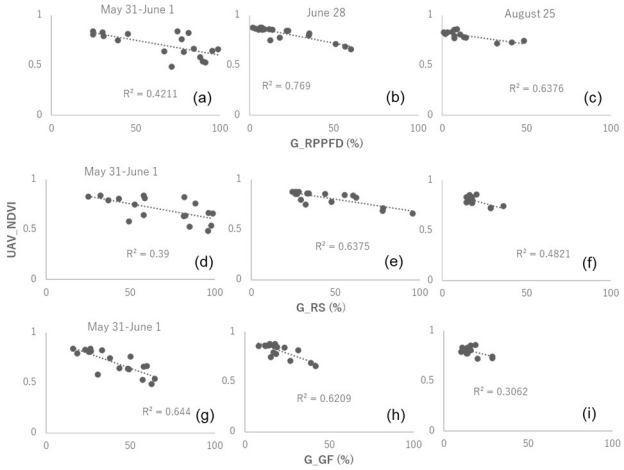

Figure 12. Comparison between UAV derived NDVI (UAV_NDVI) and ground derived relative photosynthetic photon flux density (G_RPPFD): May31-June1 (a), June 28 (b) and August 25 (c), ground derived relative solar radiation (G_RS): May31-June1 (d), June 28 (e) and August 25 (f), and ground derived gap fraction (G_GF): May31-June1 (g), June 28 (h) and August 25 (i).

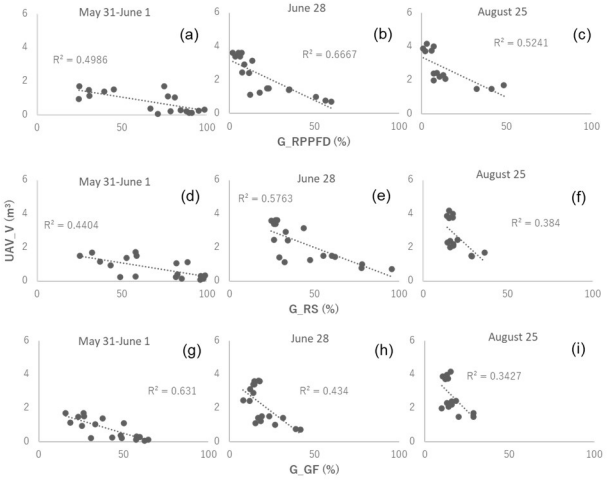

Figure 13. Comparison between UAV derived volume (UAV_V) and ground derived relative photosynthetic photon flux density (G_RPPFD): May31-June1 (a), June 28 (b) and August 25 (c), ground derived relative solar radiation (G_RS): May31-June1 (d), June 28 (e) and August 25 (f), and ground derived gap fraction (G_GF): May31-June1 (g), June 28 (h) and August 25 (i).

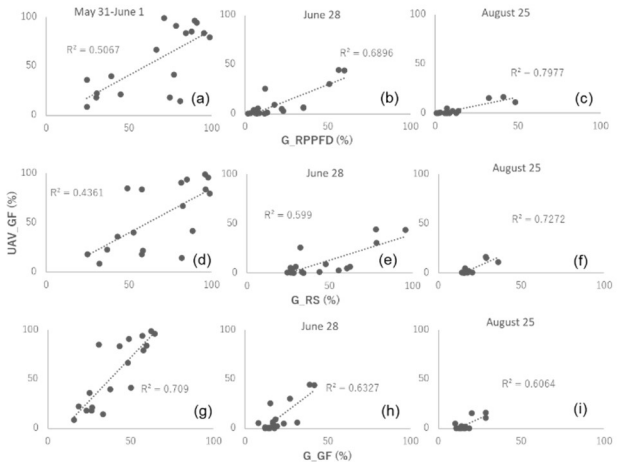

Figure 14. Comparison between UAV derived gap fraction (UAV_GF) and ground derived relative photosynthetic photon flux density (G_RPPFD): May31-June1 (a), June 28 (b) and August 25 (c), ground derived relative solar radiation (G_RS): May31-June1 (d), June 28 (e) and August 25 (f), and ground derived gap fraction (G_GF): May31-June1 (g), June 28 (h) and August 25 (i).

4. DISCUSSION

The accuracy of z values of DTM is considered to be within the acceptable range for the analysis with RMSE 4.4 cm for the north plot and 2.5 cm for the south plot at GSD of 0.40-0.43 cm. Similar value was obtained in the study of Borra-Serrano *et al*. (2019) with RMSE of 1.0-4.8 cm at GSD of 0.39-0.64 cm.

Ground derived variables: G_RPPFD, G_RS and G_GF correlated well each other (Figure 6, 7 and 8). This means that each variable represents light condition properly with seasonal variation. When gap fraction is large in an area at an early stage of vegetation growth (Figure 15a), more PPFD and solar radiation are received from the sun. As vegetation grows (Figure 15b), gap fraction is reduced due to upper leaves and stems of vegetation. PPFD and solar radiation were also reduced because leaves and stems block the sunlight.

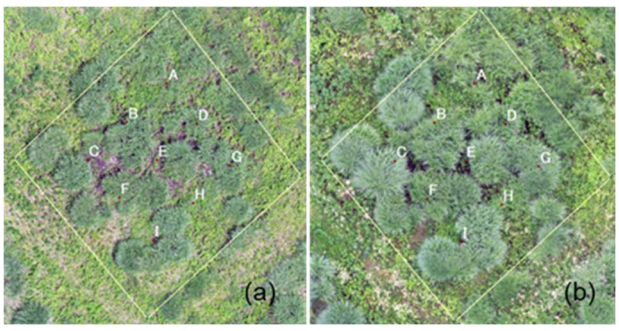

Figure 15. Early stage of vegetation growth (June 1 data in the south plot; a) and grown vegetation (June 28 data in the south plot; b).

UAV derived variables: UAV_NDVI, UAV_V and UAV_GF presented good to significant correlations between the variables with some exceptions (Figure 9, 10 and 11). UAV_NDVI and UAV_V have inverse relationship with UAV_GF. Both NDVI and volume, i.e., biomass represent the amount of vegetation. When vegetation is less in an area at an early stage of vegetation growth, larger gap fraction is presented. As vegetation grows, NDVI and biomass is increased, while gap fraction is reduced. The exceptions were observed in August 25 data between UAV_NDVI and UAV_V (Figure 9c), and between UAV_V and UAV_GF (Figure 11c). These two correlations show relatively low R^2 value of 0.32 (Figure 9c) and 0.49 (Figure 11c) respectively. Late August is around the time when the dominant species, *M. sinensis* attains its maturity. NDVI has been reported to have saturation problem that NDVI saturates over high vegetation surface and underestimate vegetation (e.g. Gu et al., 2013; Huete et al., 1997; Chen et al., 2010). It was also found out that a small patch of *M. sinensis* formed ears in the south plot. NDVI is related with greenness, however, the ears are brown color. NDVI in August 25 data might not represented the amount of vegetation accurately. For the issue of NDVI saturation, numerous papers present improved or other vegetation indices such as the red-edge triangular vegetation index (RTVI) and the modified chlorophyll absorption ratio index (MCARI2) (e.g. Haboudane et al., 2004; Chen et al., 2010) which could be applied to our data. UAV_GF seems to have similar problem. Gap fraction in the south plot already reached nearly 0 % in June 28 data, and almost all measurement displayed less than 5 % in August 25 data. On the other hand, UAV_V represents seasonal growing of vegetation properly. This could explain why UAV_NDVI and UAV_V, and UAV_V and UAV_GF in August 25 data have week association with each other.

UAV_NDVI and UAV_V were negatively associated with all ground derived variables (Figure 12 and 13), displaying overall moderate and good correlations. These were reasonable outcomes, since UAV_NDVI and UAV_V represent the amount of vegetation in each subplot, while ground derived variables represent the amount of light received at the height of 20 cm in each subplot. As vegetation grows, NDVI and vegetation volume in the subplot are increased and the amount of light at the point is decreased. NDVI in August 25 data should be treated with caution regard less of R^2 value because saturation of the value is observed (Figure 12c, 12f and 12i). UAV_V in August 25 data also needs caution, since it shows vegetation growth while ground derived variables exhibit saturation (Figure 13c, 13f and 13i).

UAV_GF presented positive and high correlations with ground derived variables (Figure 14). Although relatively low R^2 value of 0.44 (Figure 9c) was observed with G_RS in May 31-June 1 data, UAV_GF was well correlated with the rest of ground derived variables through all periods of time. In particular, since UAV_GF and G_GF access exactly the same variable and highly correlated with each other (Figure 14g, 14h and 14i), ground derived method can be replaced by UAV derived method, which has flexibility in setting up assessment points without disturbing valuable plants and site.

In conclusion, NDVI, vegetation biomass and gap fraction were estimated using time-series UAV data. UAV derived variables showed overall good correlations with ground derived variables: relative PPFD, relative solar radiation and gap fraction. Analysis of time-series UAV data revealed that UAV derived NDVI and vegetation volume were not suitable for evaluating light environment when vegetation attains its maturity. UAV derived gap fraction was most resilient to change of vegetation growth. UAV derived methods have advantage in evaluating light environment in microsite without disturbing valuable plants and would help restoring semi-natural grassland.

ACKNOWLEDGEMENTS

This research was supported by JSPS KAKENHI Grant Number 20H03015 and 21H04136. We thank Kiyohito Yoshikawa for his support in the field.

REFERENCES

Bontempo, A., Smith, J., Brandt, M., and Stoll: Evaluation of photosensitive films for light measurements in the fruiting zone of grapevine canopies, 10.5073/vitis.2018.57.159-165, 2018.

Borra-Serrano, I., De Swaef, T., Muylle, H., Nuyttens, D., Vangeyte, J., Mertens, K., Saeys, W., Somers, B., Roldan-Ruiz, I., and Lootens, P.: Canopy height measurements and non-destructive biomass estimation of Lolium perenne swards using UAV imagery, Grass and Forage Science, 74, 356-369, 10.1111/gfs.12439, 2019.

Chen, P.-f., Nicolas, T., Wang, J.-h., Philippe, V., Huang, W.-j., and Li, B.-g.: New Index for Crop Canopy Fresh Biomass Estimation, Spectroscopy and Spectral Analysis, 30, 512-517, 10.3964/j.issn.1000-0593(2010)02-0512-06, 2010.

Coops, N., Hilker, T., Wulder, M., St-Onge, B., Newnham, G., Siggins, A., and Trofymow, J.: Estimating canopy structure of Douglas-fir forest stands from discrete-return LiDAR, Trees - Structure and Function, 21, 295-310, 2007.

Flanagan, L. B., Wever, L. A., and Carlson, P. J.: Seasonal and interannual variation in carbon dioxide exchange and carbon balance in a northern temperate grassland, Global Change Biology, 8, 599-615, https://doi.org/10.1046/j.1365-2486.2002.00491.x, 2002.

Grüner, E., Astor, T., and Wachendorf, M.: Biomass Prediction of Heterogeneous Temperate Grasslands Using an SfM Approach Based on UAV Imaging, Agronomy, 9, 54, 2019.

Gu, Y., Wylie, B. K., Howard, D. M., Phuyal, K. P., and Ji, L.: NDVI saturation adjustment: A new approach for improving cropland performance estimates in the Greater Platte River Basin, USA, Ecological Indicators, 30, 1-6, https://doi.org/10.1016/j.ecolind.2013.01.041, 2013.

Haboudane, D., Miller, J. R., Pattey, E., Zarco-Tejada, P. J., and Strachan, I. B.: Hyperspectral vegetation indices and novel algorithms for predicting green LAI of crop canopies: Modeling and validation in the context of precision agriculture, Remote Sensing of Environment, 90, 337-352, https://doi.org/10.1016/j.rse.2003.12.013, 2004.

Hassan, M. A., Yang, M., Rasheed, A., Yang, G., Reynolds, M., Xia, X., Xiao, Y., and He, Z.: A rapid monitoring of NDVI across the wheat growth cycle for grain yield prediction using a multi-spectral UAV platform, Plant Science, 282, 95-103, https://doi.org/10.1016/j.plantsci.2018.10.022, 2019.

Hayashi, I., Hishinuma, Y., and Yamasawa, T.: Structure and functioning of Miscanthus sinensis grassland in Sugadaira, Central Japan, Vegetatio, 48, 17-25, 10.1007/bf00117357, 1981.

Honjo, T., Lin, T. P., and Seo, Y.: Sky view factor measurement by using a spherical camera, Journal of Agricultural Meteorology, 75, 10.2480/agrmet.D-18-00027, 2019.

Hopkinson, C. and Chasmer, L. E.: Modeling canopy gap fraction from Lidar intensity, ISPRS Workshop on Laser Scanning 2007 and SilvilLaser 2007, Espoo, Finland, September 12-14,

Huete, A. R., HuiQing, L., and Leeuwen, W. J. D. v.: The use of vegetation indices in forested regions: issues of linearity and saturation, IGARSS'97. 1997 IEEE International Geoscience and Remote Sensing Symposium Proceedings. Remote Sensing - A Scientific Vision for Sustainable Development, 3-8 Aug. 1997, 1966-1968 vol.1964, 10.1109/IGARSS.1997.609169,

Kumagai, E.: Effect of early sowing on growth and yield of determinate and indeterminate soybean (*Glycine max* (L.) Merr.) cultivars in a cool region of northern Japan, Journal of Agricultural Meteorology, advpub, 10.2480/agrmet.D-17-00009, 2018.

Lussem, U., Bolten, A., Menne, J., Gnyp, M. L., Schellberg, J., and Bareth, G.: Estimating biomass in temperate grassland with high resolution canopy surface models from UAV-based RGB images and vegetation indices, Journal of Applied Remote Sensing, 13, 10.1117/1.jrs.13.034525, 2019.

Macfarlane, C., Grigg, A., and Evangelista, C.: Estimating forest leaf area using cover and fullframe fisheye photography: Thinking inside the circle, Agricultural and Forest Meteorology, 146, 1-12, https://doi.org/10.1016/j.agrformet.2007.05.001, 2007.

Matese, A. and Di Gennaro, S. F.: Beyond the traditional NDVI index as a key factor to mainstream the use of UAV in precision viticulture, Scientific Reports, 11, 2721, 10.1038/s41598-021-81652-3, 2021.

Miura, N., Yamada, S., and Niwa, Y.: Estimation of canopy height and biomass of *Miscanthus Sinensis* in semi-natural grassland using time-series UAV data, ISPRS Ann. Photogramm. Remote Sens. Spatial Inf. Sci., V-3-2020, 497-503, 10.5194/isprs-annals-V-3-2020-497-2020, 2020.

Morsdorf, F., Kötz, B., Meier, E., Itten, K. I., and Allgöwer, B.: Estimation of LAI and fractional cover from small footprint airborne laser scanning data based on gap fraction, Remote Sensing of Environment, 104, 50-61, 2006.

Næsset, E.: Estimating timber volume of forest stands using airborne laser scanner data, Remote Sensing of Environment, 61, 246-253, 1997.

Nebara-district and Asagiri-Highlands-revitalization-committee: [Plants in Asagiri grassland] Asagirisougen-no Shokubutsu (in Japanese), 2018.

Nemoto, M.: [Japanese Nature and diversity] Nihon-rashii Shizen-to Tayosei (in Japanese), Iwanami Junior Shinsho, Iwanami Shoten, Tokyo, 222 pp.2010.

Pinag¨|, E. R., Matricardi, E. A. T., Osako, L. S., and Gomes, A. R.: Gap Fraction Estimates over Selectively Logged Forests in Western Amazon, Natural Resources, Vol.05No.16, 12, 10.4236/nr.2014.516083, 2014.

Santos, L. M. d., Ferraz, G. A. e. S., Barbosa, B. D. d. S., Diotto, A. V., Andrade, M. T., Conti, L., and Rossi, G.: Determining the Leaf Area Index and Percentage of Area Covered by Coffee Crops Using UAV RGB Images, IEEE Journal of Selected Topics in Applied Earth Observations and Remote Sensing, 13, 6401-6409, 10.1109/JSTARS.2020.3034193, 2020.

https://taisei-fc.co.jp/business/functional/environment/optoleaf-en.html, last access: March 29.

Takahashi, Y.: Semi-natural grassland ecosystem as managed nature of Japan, Reintroduction, 7, 1-9, 2019.

Tang, Y.-H., Washitani, I., Tsuchiya, T., and Iwaki, H.: Spatial heterogeneity of photosynthetic photon flux density in the canopy ofMiscanthus sinensis, Ecological Research, 4, 339-349, 10.1007/BF02348453, 1989.

Welles, J. M. and Norman, J. M.: Instrument for Indirect Measurement of Canopy Architecture, Agronomy Journal, 83, 818-825, https://doi.org/10.2134/agronj1991.00021962008300050009x, 1991.

Yuasa, Y., Bando, H., Watanabe, S., and Sei, K.: [Asagiri Highlands] Asagiri-Kougen (in Japanese), Shizuoka Kyouiku Shuppansha, Shizuoka City, 48 pp.2002.

Zhang, F., Hassanzadeh, A., Kikkert, J., Pethybridge, S. J., and van Aardt, J.: Comparison of UAS-Based Structure-from-Motion and LiDAR for Structural Characterization of Short Broadacre Crops, Remote Sensing, 13, 3975, 2021.